Published in final edited form as:
Biomaterials. 2014 December ; 35(37): 9868–9876. doi:10.1016/j.biomaterials.2014.08.038.

PET and NIR Optical Imaging Using Self-Illuminating ^{64}Cu-Doped Chelator-Free Gold Nanoclusters

Hao Hu[1,2,†], **Peng Huang**[2,†], **Orit Jacobson Weiss**[2], **Xuefeng Yan**[2], **Xuyi Yue**[2], **Molly Gu Zhang**[2], **Yuxia Tang**[2], **Liming Nie**[2,3], **Ying Ma**[2], **Gang Niu**[2], **Kaichun Wu**[1,*], and **Xiaoyuan Chen**[2,*]

[1]State Key Laboratory of Cancer Biology & Xijing Hospital of Digestive Diseases, Fourth Military Medical University, Xi'an, China

[2]Laboratory of Molecular Imaging and Nanomedicine (LOMIN), National Institute of Biomedical Imaging and Bioengineering (NIBIB), National Institutes of Health (NIH), Bethesda, MD, USA

[3]Center for Molecular Imaging and Translational Medicine, State Key Laboratory of Molecular Vaccinology and Molecular Diagnostics, School of Public Health, Xiamen University, Xiamen, China

Abstract

Self-illuminating fluorescence imaging without autofluorescence background interference has recently aroused more research interests in molecular imaging. Currently, only a few self-illuminating probes were developed, based mainly on toxic quantum dots such as CdSe, CdTe. Herein, we report a novel design of nontoxic self-illuminating gold nanocluster (^{64}Cu-doped AuNCs) for dual-modality positron emission tomography (PET) and near-infrared (NIR) fluorescence imaging based on Cerenkov resonance energy transfer (CRET). PET radionuclide ^{64}Cu was introduced by a chelator-free doping method, which played dual roles as the energy donor and the PET imaging source. Meanwhile, AuNCs acted as the energy acceptor for NIR fluorescence imaging. ^{64}Cu-doped AuNCs exhibited efficient CRET-NIR and PET imaging both *in vitro* and *in vivo*. In a U87MG glioblastoma xenograft model, ^{64}Cu-doped AuNCs showed high tumor uptake (14.9%ID/g at 18 h) and produced satisfactory tumor self-illuminating NIR images in the absence of external excitation. This self-illuminating nanocluster with non-toxicity and good biocompatibility can be employed as a novel imaging contrast agent for biomedical applications, especially for molecular imaging.

Corresponding authors: Kaichun Wu, Address: Xijing Hospital of Digestive Diseases, Fourth Military Medical University, 127 West Changle Road, Xi'an, 710032, China; Tel: + 86 29 84771502; Fax: + 86 29 82539041; kaicwu@fmmu.edu.cn. Xiaoyuan Chen, Address: Laboratory of Molecular Imaging and Nanomedicine (LOMIN), National Institute of Biomedical Imaging and Bioengineering (NIBIB), National Institutes of Health, 35A Convent Dr GD937, Bethesda, MD 20892-3759, Tel: 301-451-4246, Fax: 301-480-1613, shawn.chen@nih.gov.
[†]These authors contributed equally.

1. Introduction

Self-illuminating fluorescence imaging is a newly developed imaging technique, overcoming several shortcomings of traditional fluorescence imaging. It has many distinguished imaging advantages, such as: i) no need of excitation from external illumination sources to fluoresce, resulting in no interference of strong background autofluorenscence [1, 2], and ii) no issue of excitation attenuation caused by photons absorption/scattering in bio-tissue transmission [3], which serves extremely important for *in vivo* imaging, as most imaging targets are non-superficial. So far, only a few self-illuminating fluorescence probes are designed and constructed based on three different energy transfer mechanisms such as bioluminescence resonance energy transfer (BRET), chemiluminescence resonance energy transfer (CLRET) and Cerenkov resonance energy transfer (CRET). Quantum dots (QDs), due to their high quantum yield, tunable emission peaks, long fluorescence lifetimes, and negligible photobleaching, have been employed as the energy transfer acceptor. For example, So *et al*. described self-illuminating QDs based on BRET, in which the bioluminescence energy of the luciferase-catalyzed oxidation of coelenterazine was transferred to the CdSe/ZnS QDs [2]. Zhang *et al*. reported another CLRET-CdSe/ZnS QDs methodology for *in vivo* myeloperoxidase (MPO) [4]. Recently, we constructed CRET-based self-illuminating QDs. In this system, Cerenkov radiation of ^{64}Cu was transferred to excite the CdSe/ZnS QDs [5]. However, self-illuminating QDs are limited for further biomedical applications because most QDs contain heavy metal elements (such as Cd^{2+}, Pb^{2+}, *etc*.) and tend to self-aggregate inside living cells [6-8]. The cytotoxicity of the released heavy metal ions in biological systems and potential environmental hazard of these ions always hinder their practical applications [9, 10]. Therefore, it is highly desirable to develop novel self-illuminating systems with non-toxicity and good biocompatibility for further biomedical applications, especially in molecular imaging and therapy.

Recently, noble metal nanoclusters (such as gold nanoclusters (AuNCs)), due to their high fluorescence, good photostability, non-toxicity, excellent biocompatibility and water solubility, have aroused great interest in the development of new types of luminescent probes [11-18]. More importantly, these nanoclusters are usually prepared by a biomimetic synthesis method using naturally functional macromolecules (proteins, peptides, and enzymes *etc*.) as templates, which provides the nanoclusters with good colloidal stability and solubility in biological systems and avoid them from undesired or nonspecific binding [11, 17, 19]. Meanwhile, the macromolecules provide bioactive functional groups, such as $-NH_2$ and −COOH, which can be used for further surface functionalization [20-22]. Therefore, metal nanoclusters are a good choice as energy transfer acceptors for developing novel self-illuminating fluorescent probes.

Herein, we strategically designed and prepared self-illuminating ^{64}Cu-doped gold nanoclusters (^{64}Cu-doped AuNCs) for dual-modality positron emission tomography (PET) and near infrared (NIR) imaging. The radioactive ^{64}Cu plays dual roles as both the energy donor to excite AuNCs and the positron-emitting radionuclide (tracer) for PET imaging, while AuNCs act as the energy acceptor for self-illuminating NIR fluorescence imaging (**Scheme 1**). A novel chelator-free ^{64}Cu doping method was developed for rapid radiolabeling of the AuNCs (within 1 h). The as-prepared ^{64}Cu-doped AuNCs exhibited

good stability, water dispersibility and solubility *in vitro*, and noncytotoxicity and good biocompatibility *in vivo*. In a U87MG glioblastoma xenograft model, ^{64}Cu-doped AuNCs displayed satisfactory synergistic dual-modality PET and self-illuminating NIR tumor imaging.

2. Material and methods

2.1. Chemicals

All chemicals were purchased from Sigma-Aldrich Chemical Co. and used without further purification. Water was purified with Milli-Q plus system (Millipore Co., Bedford, MA), and the resistivity was kept to be over 18 MΩ cm.

2.2. Preparation of the HSA-AuNCs and ^{64}Cu-doped AuNCs

The procedure for synthesizing HSA-AuNC synthesis was similar to that for BSA-AuNCs. Briefly, the aqueous $HAuCl_4$ solution (5 mL, 10 mM) was added to HSA solution (5 mL, 50 mg/mL) under vigorous stirring. Five min later, NaOH solution (0.5 mL, 1 M) was introduced, and the pH changed to ~12. The reaction was allowed to proceed under vigorous stirring at 37 °C for 12 h. The reaction mixture was kept in the refrigerator (4 °C) in the dark for further use.

For ^{64}Cu doping, all the solutions used were de-gassed for 40 min before use, and the AuNC solution was washed to pH 8~9 by PBS. 5-6 mCi $^{64}CuCl_2$ was added to 1 mL of AuNCs solution under stirring for 5 min. Then, 10 μL of hydrazine hydrate was added and stirring continued for another 40 min at room temperature. Purification was done in a PD-10 column washed with 0.1% Na-ascorbate in PBS. Radiochemical purity was measured by instant thin layer chromatography (ITLC) plates using 0.1 M citric acid as eluent. 1-10% (molar ratio) Cu-doped AuNCs were prepared with the same procedure.

2.3. Characterization of ^{64}Cu-doped AuNCs

Transmission electron microscope (TEM) images were acquired using a JEM-2010 (JEOL Ltd., Japan) operated at an accelerating voltage of 200 kV. UV-Vis-NIR spectra were measured on a Genesys 10S UV-Vis spectrophotometer (Thermo Scientific, Waltham, MA) using quartz cuvettes with an optical path of 1 cm. Fluorescence emission spectra were recorded on an F-7000 fluorescence spectrophotometer (Hitachi, Tokyo, Japan). CD spectra (190–300 nm) were recorded on a Jasco J-815 spectropolarimeter.

2.4. Cell culture and animal model

U87MG glioblastoma cell line was bought from ATCC and cultured in EMEM containing 10% fetal bovine serum (Gibco, Grand Island, NY) and incubated at 37 °C in a humidified 5% CO_2 incubator. All animal work was performed following a protocol approved by the National Institutes of Health Clinical Center Animal Care and Use Committee (NIH CC/ACUC). Athymic nude mice purchased from Harlan (Indianapolis, IN) were subcutaneously implanted with 5×10^6 U87MG cells in the right front flank. *In vivo* imaging was performed 3 weeks after the inoculation when the tumor volume reached around 75 mm^3.

2.5. CKK8 safety assay

5×10^3 cells per well were seeded in 96-well plate and incubated with AuNCs or decayed ^{64}Cu-doped AuNCs for 24 h at different concentrations (100, 50, 25, 12.5 and 6.25 μM). Then the CKK8 agent (Dojindo Laboratories, Japan) was added to each well and incubated for 2 h, the absorbance at 450 nm was measured. Cell viability was normalized by control group without any treatment.

2.6. Cell uptake and FACS

50 μM AuNCs or decayed ^{64}Cu-doped AuNCs were co-incubated with U87MG cells at 37 °C in a humidified 5% CO_2 incubator. At different time points (0.5, 1, 2, 4, and 18 h), the uptake of AuNCs was analyzed by an Acurri C6 Flow Cytometer (BD Biosciences). The untreated cells were served as a control. The microscopic observation of internalization was carried out at 6 h after incubation. The nucleus was counter stained with DAPI. The images were captured by an inverted fluorescence microscope (Olympus IX81, Japan).

2.7. MicroPET imaging and Biodistribution study

The U87MG tumor-bearing mice were anesthetized with isoflurane and were injected with 100 μL 7.4 MBq (200 μCi) ^{64}Cu-doped AuNCs intravenously. All PET scans were performed on an Inveon small-animal PET scanner (Siemens, Erlangen, Germany) at indicated time point post injection. The images were collected for 10 min. For each PET scan, 3-dimensional volumes of interest (VOIs) were drawn over the tumor and muscle on decay-corrected whole-body coronal images and analyzed by Inveon Research Workplace (Siemens). At the endpoint of experiment, the mice were sacrificed and interested organs were harvested, weighted and the radioactivity was measured in a Beckman 8000 gamma counter (Beckman, Brea, CA). Standards were prepared and the organ uptake was calculated as percent of injected dose/gram of tissue (%ID/g).

2.8. *In vitro* and *in vivo* self-illuminating fluorescence imaging

For *in vitro* self-illuminating fluorescence imaging, 11.1 MBq (300 μCi) of $^{64}CuCl_2$ and ^{64}Cu-doped AuNCs were imaged by an IVIS Lumina II small animal imaging system (Caliper Life Sciences, Hopkinton, MA). The images were taken under different emission filter sets (no filter, <510 nm, >590 nm, 515-575 nm, 575-650 nm, 695-770 nm and 810-885 nm), with the exposure time of 5 min, f/top = 1, binning = 4. For *in vivo* imaging, after the tumor-bearing mice were transferred to the light-tight chamber of IVIS imaging system, the images were taken with three different emission filter sets (no filter, <510 nm and >590 nm).The acquisition conditions were: exposition time 10 min, f/top = 1, binning = 4. All the images were analyzed by the Living Image 3.0 software (Caliper Life Science) and the signal was represented as photons per second per centimeter square per steradian ($p/s/cm^2/sr$).

3. Results and discussion

3.1. Characterization of Cu-doped AuNCs

Fluorescent AuNCs were prepared by a human serum albumin (HSA)-directed, solution-phase, biomimetic synthetic method. As shown in **Figure 1a** and **b**, both AuNCs and Cu-doped AuNCs (1% Cu) are spherical. After Cu-doping, the size of AuNCs is increased from 0.93 ± 0.25 to 2.56 ± 0.50 nm (**Figure 1c** and **d**). UV-vis absorbance and fluorescence emission spectra of Cu-doped AuNCs (1% Cu) are shown in **Figure 1e**. The Cu-doped AuNCs (1% Cu) has one characteristic absorption peak at 280 nm, which is assigned to the $\pi \rightarrow \pi^*$ transition of the aromatic amino acid residues of HSA. Under the excitation at 514 nm, Cu-doped AuNCs (1% Cu) exhibits maximum emission at ~667 nm. In addition, the structure conformation of pure HSA and Cu-doped AuNCs (1% Cu) is also investigated using a circular dichroism (CD) spectropolarimeter (**Figure 1f**). Pure HSA shows a positive absorption band at 190 nm and two negative absorption bands at 209 and 222 nm. With the formation of Cu-doped AuNCs (1% Cu), the positive peak at 190 nm ascends and the two negative peaks display slight blue shifts to 205 and 221 nm, respectively.

3.2. The effects of different doping concentration of Cu

The fluorescence intensity of Cu-doped AuNCs gradually deceases with the increase of Cu-doping ratio (**Figure 2a** and **Supplementary Figure S1a**). Cu-doped AuNCs display good stability in water, PBS and serum (**Figure 2b, c** and **Supplementary Figure S1b**). More importantly, both AuNCs and Cu-doped AuNCs (1% Cu) exhibit higher photostability than conventional fluorescent dyes (**Figure 2d**).

3.3. Dual imaging potentials of ^{64}Cu-doped AuNCs

Next, we prepared the Cu-doped AuNCs with “hot” copper using the same procedure. After the implementation of hydrazine hydrate reduction, almost all the ^{64}Cu was reduced and doped onto the AuNCs (**Supplementary Figure S2**). To analyze the ^{64}Cu doping location, we used HSA as control. The instant thin layer chromatography (ITLC) results showed that HSA alone cannot be labeled by ^{64}Cu with the same doping method (**Supplementary Figure S3**), suggesting that ^{64}Cu was doped on the AuNCs, rather than on HSA. We then examined the NIR and PET imaging capability of ^{64}Cu-doped AuNCs. 5.5 MBq (150 μCi, 250 μL, 5 mM) ^{64}Cu-doped AuNCs were imaged by PET and fluorescence imaging, respectively. The ^{64}Cu-doped AuNCs exhibited high PET signal and displayed comparable NIR imaging performance to the corresponding AuNCs under the same external excitation (**Figure 3a**). This result demonstrates that ^{64}Cu doping provides AuNCs with PET imaging ability and the trace amount of doped ^{64}Cu had no obvious impairment to the NIR fluorescence of AuNCs. As Cerenkov radiation is most intense at high frequencies (ultraviolet/blue area) [23], which overlaps exactly with the absorption spectrum of the AuNCs, the CRET would happen within ^{64}Cu-doped AuNCs. In order to reveal CRET and evaluate subsequent self-illumination, multi-spectra imaging analysis was carried out with IVIS system. 11.1 MBq (300 μCi) ^{64}Cu-doped AuNCs and $^{64}CuCl_2$ were imaged with serial filter sets (no filter, < 515 nm, > 590 nm, 515-575 nm, 575-650 nm, 595-770 nm and 810-875 nm). Each filter only allows certain wavelength of light to pass (**Figure 3b**). In the

no filter group, which collected all the signals, the ^{64}Cu-doped AuNCs showed an intensity of 1.6- that of $^{64}CuCl_2$. A reasonable explanation for this excessive intensity is that AuNCs yield additional signals under the excitation of Cerenkov radiation from ^{64}Cu. Indeed, with the filter of > 590 nm, which covers most of the emission spectrum of ^{64}Cu-doped AuNCs, we recorded an intensity 2.7 times that of $^{64}CuCl_2$ (**Figure 3c**). Moreover, with filter sets of 575-650 nm and 695-770 nm, which contain parts of the emission spectrum of AuNCs, the intensities of ^{64}Cu-doped AuNCs were 1.5-fold and 4.3-fold that of $^{64}CuCl_2$ (**Figure 3d**). In contrast, with the filter < 510 nm, which is believed to be the main emission area of Cerenkov radiation, the ^{64}Cu-doped AuNCs showed lower intensity than that of $^{64}CuCl_2$. This is reasonable, as a portion of the Cerenkov radiation was transferred from ^{64}Cu to AuNCs (**Figure 3d**).

3.4. *In vivo* CRET imaging of ^{64}Cu-doped AuNCs

Cerenkov radiation itself is not suitable for *in vivo* studies due to its short wavelength [5, 23]. However by CRET, the energy from Cerenkov radiation can be transferred to AuNCs, which have a longer emission wavelength and deeper tissue penetration. To identify the imaging potential of ^{64}Cu-doped AuNCs *in vivo*, we chose to utilize the U87MG glioblastoma xenograft model, as cell uptake and flow cytometry assay identified high uptake of Cu-doped AuNCs on this cell line, CKK8 viability assay disclosed no obvious cytotoxicity to the U87MG cells (**Figure 4a-c**). U87 Tumor-bearing mice were given 7.4 MBq (200 μCi) of ^{64}Cu-doped AuNCs intravenously and then sequentially scanned by IVIS with 3 different filter sets (no filter, > 590 nm and < 510 nm). The whole-body IVIS images showed an enhanced tumor uptake of ^{64}Cu-doped AuNCs after injection, reaching maximum at 8 h post injection followed by a decrease in intensity due to isotope decay (**Figure 5a**). Importantly, the CRET-NIR imaging (measured by > 590 nm filter) showed satisfactory tumor uptake compared to Cerenkov imaging (measured by filter < 510 nm), in which tumor uptake can barely be detected under the same intensity scale bar (**Supplementary Figure S4**). To compare the intensities between the 3 filters, regions of interests (ROIs) were drawn over the tumors. The intensities of CRET-NIR were slightly lower than those of the no filter group, accounting for around 4/5 of the total signal intensities. This is because the lower wavelength of Cerenkov radiation was deducted from the total intensity. On the contrary, only about 1/7 of the total signal was coming from Cerenkov radiation (**Figure 5b**). These encouraging results further confirmed the *in vivo* imaging potentials of self-illuminating ^{64}Cu-doped AuNCs and demonstrated that CRET-NIR was the main luminescent contributor to self-illumination, compared with Cerenkov radiation alone.

3.5. *In vivo* PET imaging of ^{64}Cu-doped AuNCs

The simultaneous PET imaging is another advantage of self-illuminating ^{64}Cu-doped AuNC. Complementary to NIR imaging, PET has infinite penetration and provides more quantitative information [24, 25]. The PET imaging was taken immediately after the IVIS scan. The decay-corrected whole-body PET images and 3D reconstruction showed high tumor to normal contrast (**Figure 6a** and **Supplementary Movie S1**). Quantitative three-dimensional volumes of interest (VOIs) analysis identified about 6.9 percent of injected dose/gram of tissue (%ID/g) tumor uptake of ^{64}Cu-doped AuNCs at 1 h post injection,

which increased to 14.9 %ID/g and 15.2 %ID/g at 18 h and 24 h, respectively (**Figure 6b**). The tumor to muscle ratios (T/NT) also increased from 5.8 at 1 h post injection, to a peak of 28.4 at 18 h post injection (**Figure 6c**). The imaging discrepancy between PET and previous self-illuminating imaging may be attributed to the isotope decay. The %ID/g value is a decay-corrected value in PET imaging. Therefore, we recorded an increased %ID/g value of tumor, while the absolute radioactivity decreased because of isotope decay. In self-illuminating imaging, ^{64}Cu was the energy donor. The luminescent intensity is thus positively correlated with its radioactivity. This is why we recorded maximum tumor uptake at 18 h time point in PET, but at 8 h time point in self-illuminating imaging. Actually, if we calculate and plot the images without decay correction, the pattern of PET would be consistent with IVIS imaging results (**Supplementary Figure S5**).

3.6. The correlation between CRET and PET signals

To further understand the correlation among PET, CRET-NIR (> 590 nm) and Cerenkov radiation (< 510 nm), we compared their signal intensities. At 24 h post injection, the tumor and five other organs were extracted, and acquired by IVIS and PET imaging respectively (**Figure 7a, b**, and **Supplementary Figure S6**). The ROI measurement displayed good linear correlation between PET and total signal (no filter, $r^2 = 0.9340$, **Figure 7c**), and PET and CRET-NIR signal (> 590 nm; $r^2 = 0.9687$, **Figure 7d**). In contrast, a weaker linear correlation was found between PET signals and Cerenkov radiation (< 510 nm; $r^2 = 0.7616$, **Figure 7e**). As we know Cerenkov radiation is linearly correlated with the PET activity [26, 27], these results demonstrate that a portion of the energy of Cerenkov radiation serves to excite AuNCs in ^{64}Cu-doped AuNCs. Furthermore, high linear correlation suggests that the self-illumination intensity of ^{64}Cu-doped AuNCs can be applied as an alternative indicator of PET signal. In addition, organ distribution results indicate that the liver and kidneys may be responsible for the route of clearance of ^{64}Cu-doped AuNCs (**Figure 7f**). Histological examination showed no obvious organ damage at 1 day and 7 days after injection of ^{64}Cu-doped AuNCs (**Supplementary Figure S7**)

4. Conclusion

In summary, we developed a novel self-illuminating gold nanocluster, ^{64}Cu-doped AuNCs, for dual-modality PET and CRET-NIR fluorescence imaging. To the best of our knowledge, it is the first time that noble metal nanoclusters have been reported as energy transfer acceptors for multimodality imaging. The ^{64}Cu-doped AuNCs we developed have the following features: 1) both PET and self-illuminating NIR imaging capabilities; 2) *in vivo* self-illumination, converting short wavelengths of Cerenkov radiation into longer wavelengths; 3) small size, high solubility and stability in aqueous media, and 4) non-toxicity and good biocompatibility. These self-illuminating nanoclusters provide novel biomedical research tools, especially for molecular imaging and cancer therapy.

Supplementary Material

Refer to Web version on PubMed Central for supplementary material.

Acknowledgments

This work was supported, in part, by the Intramural Research Program (IRP) of the NIBIB, NIH, the National Key Basic Research Program (973 Project) (2010CB933901, 2013CB733802, 2014CB744503) and the National Natural Science Foundation of China (No.81090270, No.81090273 and No.81370585). We also thank Dr. Jie Lu, Dale Kiesewetter, and Andrea Balbo for their technical support.

References

[1]. Frangioni JV. Self-illuminating quantum dots light the way. Nat Biotechnol. 2006; 24:326–8. [PubMed: 16525407]

[2]. So MK, Xu C, Loening AM, Gambhir SS, Rao J. Self-illuminating quantum dot conjugates for in vivo imaging. Nat Biotechnol. 2006; 24:339–43. [PubMed: 16501578]

[3]. Wu Q, Chu M. Self-illuminating quantum dots for highly sensitive in vivo real-time luminescent mapping of sentinel lymph nodes. Int J Nanomed. 2012; 7:4531. vol 7, pg 3443, 2012.

[4]. Zhang N, Francis KP, Prakash A, Ansaldi D. Enhanced detection of myeloperoxidase activity in deep tissues through luminescent excitation of near-infrared nanoparticles. Nat Med. 2013; 19:500–5. [PubMed: 23455711]

[5]. Sun X, Huang X, Guo J, Zhu W, Ding Y, Niu G, et al. Self-illuminating ^{64}Cu-doped CdSe/ZnS nanocrystals for *in vivo* tumor imaging. J Am Chem Soc. 2014; 136:1706–9. [PubMed: 24401138]

[6]. Weng J, Ren J. Luminescent quantum dots: a very attractive and promising tool in biomedicine. Curr Med Chem. 2006; 13:897–909. [PubMed: 16611074]

[7]. Huang P, Lin J, Wang X, Wang Z, Zhang C, He M, et al. Light-triggered theranostics based on photosensitizer conjugated carbon dots for simultaneous enhanced fluorescence imaging and photodynamic therapy. Adv Mater. 2012; 24:5104–10. [PubMed: 22718562]

[8]. Huang P, Li Z, Lin J, Yang D, Gao G, Xu C, et al. Photosensitizer-conjugated magnetic nanoparticles for *in vivo* simultaneous magnetofluorescent imaging and targeting therapy. Biomaterials. 2011; 32:3447–58. [PubMed: 21303717]

[9]. Hardman R. A toxicologic review of quantum dots: Toxicity depends on physicochemical and environmental factors. Environ Health Persp. 2006; 114:165–72.

[10]. Huang P, Bao L, Yang D, Gao G, Lin J, Li Z, et al. Protein-directed solution-phase green synthesis of BSA-conjugated M_xSe_y (M= Ag, Cd, Pb, Cu) nanomaterials. Chem Asian J. 2011; 6:1156–62. [PubMed: 21341374]

[11]. Luo Z, Zheng K, Xie J. Engineering ultrasmall water-soluble gold and silver nanoclusters for biomedical applications. Chem Commun (Camb). 2014; 50:5143–55. [PubMed: 24266029]

[12]. Xie J, Zheng Y, Ying JY. Protein-directed synthesis of highly fluorescent gold nanoclusters. J Am Chem Soc. 2009; 131:888–9. [PubMed: 19123810]

[13]. Li M, Yang DP, Wang X, Lu J, Cui D. Mixed protein-templated luminescent metal clusters (Au and Pt) for H_2O_2 sensing. Nanoscale Res Lett. 2013; 8:182. [PubMed: 23601828]

[14]. Zheng J, Nicovich PR, Dickson RM. Highly fluorescent noble-metal quantum dots. Annu Rev Phys Chem. 2007; 58:409–31. [PubMed: 17105412]

[15]. Lin J, Zhou Z, Li Z, Zhang C, Wang X, Wang K, et al. Biomimetic one-pot synthesis of gold nanoclusters/nanoparticles for targeted tumor cellular dual-modality imaging. Nanoscale Res Lett. 2013; 8:1–7. [PubMed: 23279756]

[16]. Huang P, Lin J, Wang S, Zhou Z, Li Z, Wang Z, et al. Photosensitizer-conjugated silica-coated gold nanoclusters for fluorescence imaging-guided photodynamic therapy. Biomaterials. 2013; 34:4643–54. [PubMed: 23523428]

[17]. Zhang C, Zhou Z, Qian Q, Gao G, Li C, Feng L, et al. Glutathione-capped fluorescent gold nanoclusters for dual-modal fluorescence/X-ray computed tomography imaging. J Mater Chem B. 2013; 1:5045–53.

[18]. Zhang XD, Chen J, Luo Z, Wu D, Shen X, Song SS, et al. Enhanced tumor accumulation of sub-2 nm gold nanoclusters for cancer radiation therapy. Adv Healthc Mater. 2014; 3:133–41. [PubMed: 23873780]

[19]. Xavier PL, Chaudhari K, Baksi A, Pradeep T. Protein-protected luminescent noble metal quantum clusters: an emerging trend in atomic cluster nanoscience. Nano Rev. 2012; 3 doi: 10.3402/nano.v3i0.14767.

[20]. Wang YL, Chen JJ, Irudayaraj J. Nuclear Targeting Dynamics of Gold Nanoclusters for Enhanced Therapy of HER2(+) Breast Cancer. Acs Nano. 2011; 5:9718–25. [PubMed: 22053819]

[21]. Retnakumari A, Setua S, Menon D, Ravindran P, Muhammed H, Pradeep T, et al. Molecular-receptor-specific, non-toxic, near-infrared-emitting Au cluster-protein nanoconjugates for targeted cancer imaging. Nanotechnology. 2010; 21

[22]. Retnakumari A, Setua S, Menon D, Ravindran P, Muhammed H, Pradeep T, et al. Molecular-receptor-specific, non-toxic, near-infrared-emitting Au cluster-protein nanoconjugates for targeted cancer imaging. Nanotechnology. 2010; 21:055103. [PubMed: 20023317]

[23]. Mitchell GS, Gill RK, Boucher DL, Li C, Cherry SR. In vivo Cerenkov luminescence imaging: a new tool for molecular imaging. Philos Trans A Math Phys Eng Sci. 2011; 369:4605–19. [PubMed: 22006909]

[24]. Zhao Y, Sultan D, Detering L, Cho S, Sun G, Pierce R, et al. Copper-64-alloyed gold nanoparticles for cancer imaging: improved radiolabel stability and diagnostic accuracy. Angew Chem Int Ed Engl. 2014; 53:156–9. [PubMed: 24272951]

[25]. Chen F, Ellison PA, Lewis CM, Hong H, Zhang Y, Shi S, et al. Chelator-free synthesis of a dual-modality PET/MRI agent. Angew Chem Int Ed Engl. 2013; 52:13319–23. [PubMed: 24166933]

[26]. Xu YD, Liu HG, Cheng Z. Harnessing the Power of Radionuclides for Optical Imaging: Cerenkov Luminescence Imaging. J Nucl Med. 2011; 52:2009–18. [PubMed: 22080446]

[27]. Ruggiero A, Holland JP, Lewis JS, Grimm J. Cerenkov luminescence imaging of medical isotopes. J Nucl Med. 2010; 51:1123–30. [PubMed: 20554722]

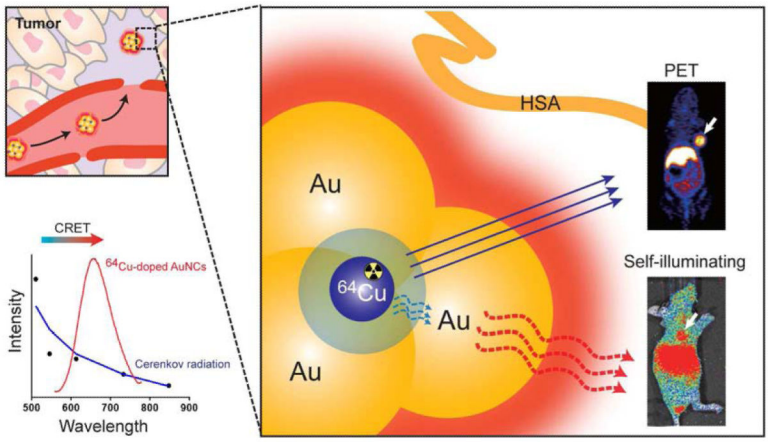

Scheme 1.

Self-illuminating 64Cu-doped gold nanoclusters (64Cu-doped AuNCs) for in vivo synergistic dual-modality positron emission tomography (PET) and self-illuminating near infrared (NIR) imaging. PET radionuclide 64Cu plays dual roles as the energy donor to excite AuNCs as well as the positron-emitting radionuclide (tracer) for PET imaging. The AuNCs act as the energy acceptor for self-illuminating NIR fluorescence imaging. HSA, human serum albumin.

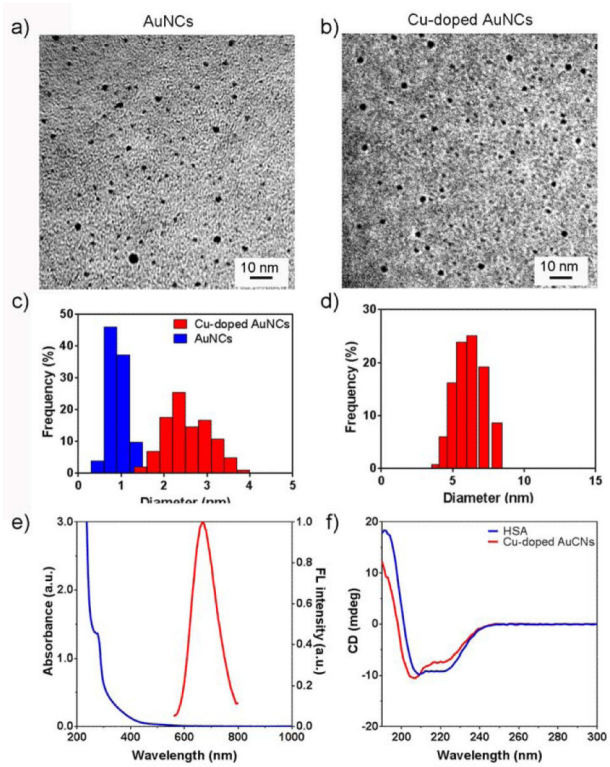

Figure 1.

TEM images of AuNCs (a) and Cu-doped AuNCs (1% Cu); (b). The scale bar is 10 nm; (c) Histogram of size distribution of Cu-doped AuNCs (1%) and AuNCs calculated from TEM images; (d) hydrodynamic diameter (HD) of Cu-doped AuNCs (1%) in PBS, measured by dynamic light scattering (DLS); (e) UV-vis absorbance and fluorescence emission spectrum of Cu-doped AuNCs (1% Cu); (f) CD spectra of pure HSA and Cu-doped AuNCs (1% Cu).

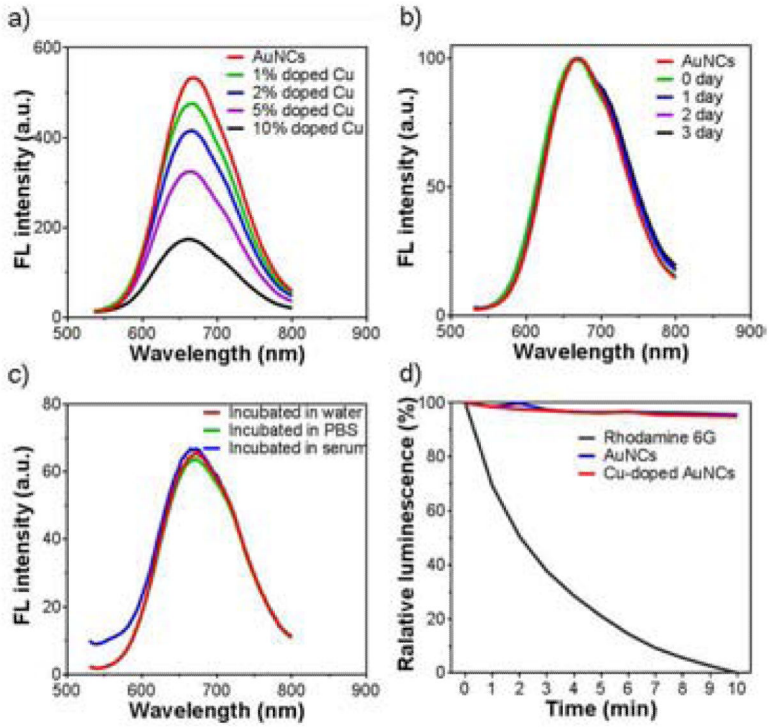

Figure 2.

(a) Fluorescence emission spectra of Cu-doped AuNCs in PBS (pH = 7.4) at different Cu-doping ratio. (b) Fluorescence emission spectra of Cu-doped AuNCs (1%) in PBS (pH = 7.4) at different days. (c) Fluorescence emission spectra of Cu-doped AuNCs (1%) in different solvents after 24 h incubation. (d) Photo-stability of AuNCs and Cu-doped AuNCs (1%) by compared with and Rhodamine 6G.

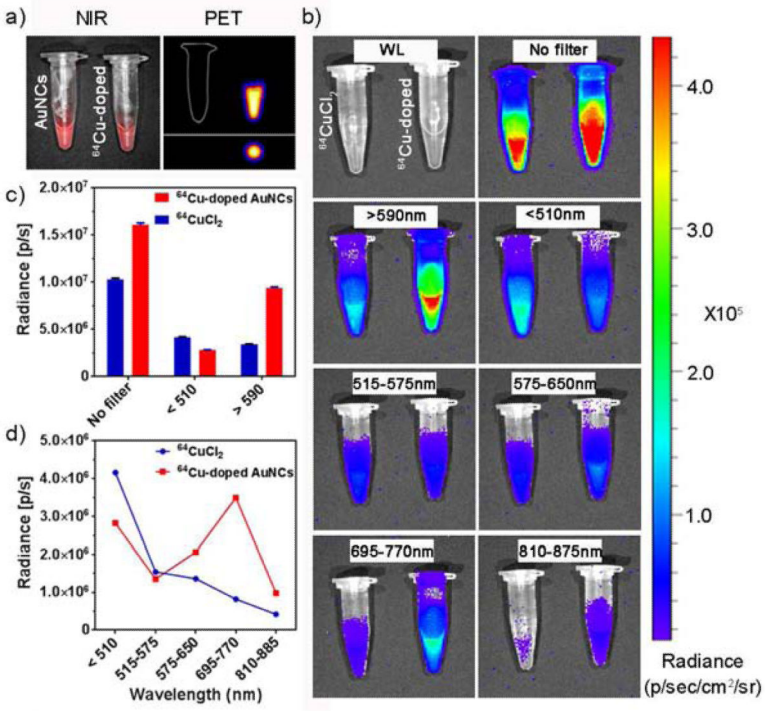

Figure 3.

(a) NIR and PET images of AuNCs (left) and ^{64}Cu-doped AuNCs (right). Under excitation, both AuNCs and ^{64}Cu-doped AuNCs showed NIR fluorescence, while only ^{64}Cu-doped AuNCs were PET positive; (b) Images of $^{64}CuCl_2$ (left) and self-illuminating ^{64}Cu-doped AuNCs in the absence of external excitation (right); WL, white light; no filter, all wavelengths were collected; < 510, wavelengths below 510 allow to pass; > 590 nm, wavelengths above 590 allow to pass; 515-575 nm, 575-650 nm, 695-770 nm and 810-875 nm, only allow the wavelengths indicated to pass; (c) Intensity comparison of $^{64}CuCl_2$ and ^{64}Cu-doped AuNCs at no filter, < 510nm and > 590 nm filter; (d). intensity changes of $^{64}CuCl_2$ and ^{64}Cu-doped AuNCs at different filter sets.

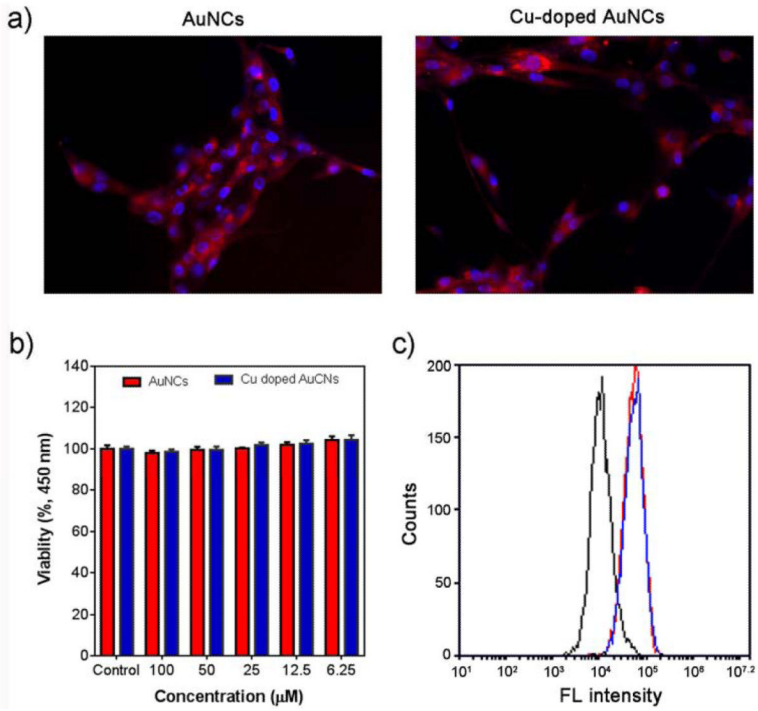

Figure 4.

(a) U87MG cell uptake after 6 h incubation with AuNCs and decayed Cu-doped AuNCs; (b) CCK8 safety assay of AuNCs and decayed Cu-doped AuNCs; (c) Flow cytometry quantification of cell uptake at 6 h; Black, control cell; Red, AuNCs; Blue, decayed Cu-doped AuNCs.

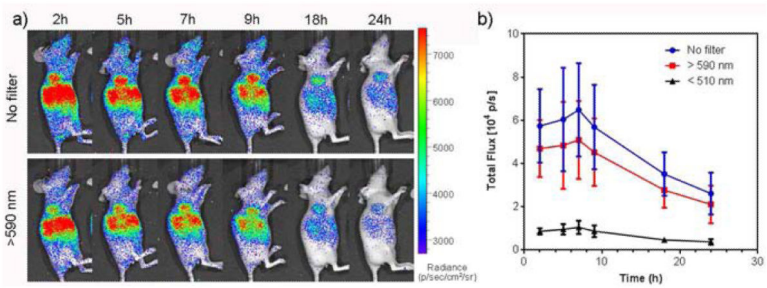

Figure 5.

(a) Representative self-illuminating NIR images of ^{64}Cu-doped AuNCs on U87MG glioblastoma xenografted mice. Images were acquired at 1, 3, 8, 10, 18 and 24 h post-injetcion. No filters, > 590 nm and < 510 nm (see supplementary files) filters sets were used; (b) Dynamic changes of self-illuminating intensity of tumor, measured by ROIs;

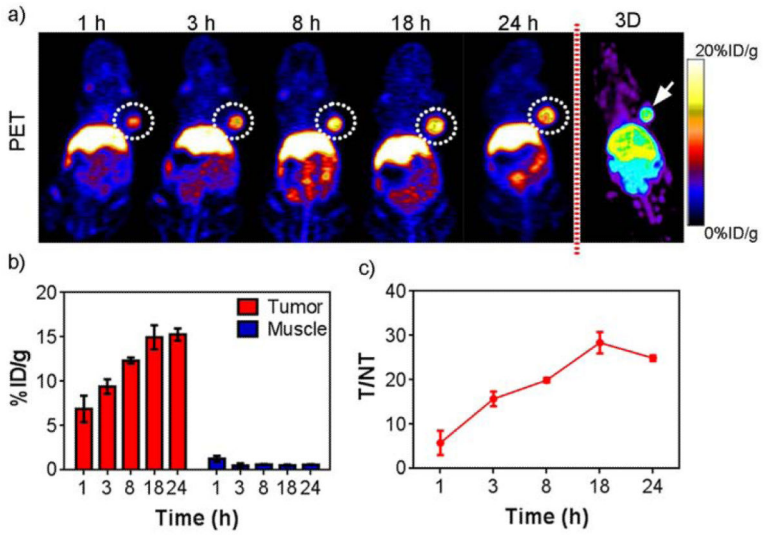

Figure 6.

(a) Representative PET and three-dimensional (3D) PET reconstruction images of ^{64}Cu-doped AuNCs on U87MG glioblastoma bearing mice. Images were acquired at 1, 3, 8, 18 and 24 h. (b) Tumor and muscle uptake of ^{64}Cu-doped AuNCs, measured by VOIs. Date were average decay-corrected to the time of injection, presented as %ID/g; (c) Tumor/muscle (T/NT) ratio at different time point; Tumor was marked by dashed circles or white arrow; n=4.

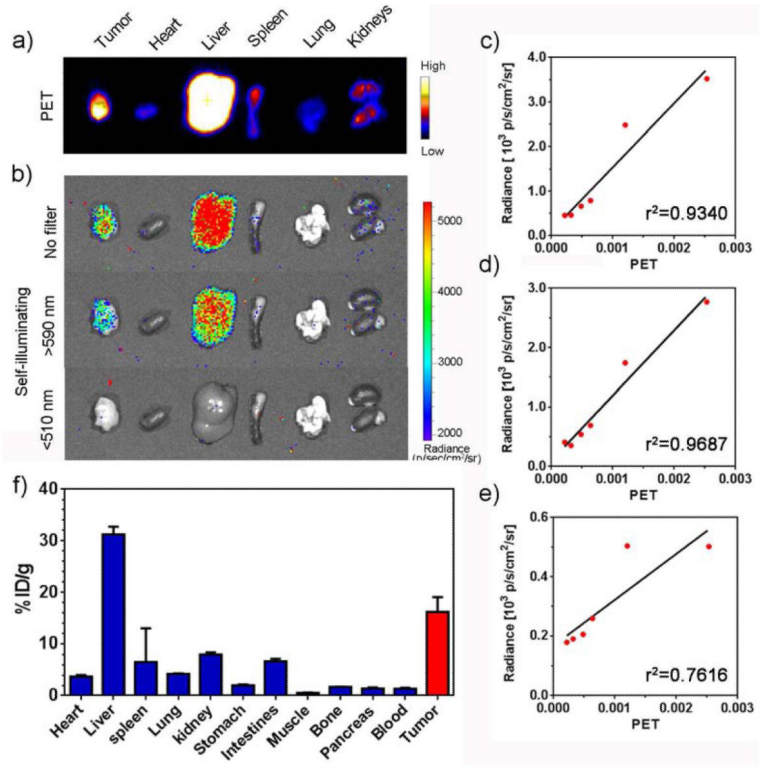

Figure 7.

(a) *Ex-vivo* PET images of major organs at 24 h; (b) *Ex-vivo* self-illuminating NIR images of major organs at 24 h (no filter, < 510 nm and > 590 nm filter sets); (c) Linear correlation between PET and self- illuminating (no filter) intensities, r^2=0.9340; (d) Linear correlation between PET and CRET-NIR (> 590 nm filter) intensities, r^2=0.9687; (e) Linear correlation between PET and Cerenkov Radiation (< 510 nm filter) intensities, r^2=0.7616; (f) Biodistribution of ^{64}Cu-doped AuNCs at 24 h, calculated by γ-counter, n=4.